ELSEVIER

Catalysis Today 82 (2003) 275–281

CATALYSIS TODAY

www.elsevier.com/locate/cattod

Co-current and counter-current modes for water gas shift membrane reactor

Angelo Basile*, Luca Paturzo, Fausto Gallucci

Institute on Membrane Technology, ITM-CNR, c/o University of Calabria, Via P. Bucci, Cubo 17/C, 87030 Rende, CS, Italy

Abstract

In this study the performances of a membrane reactor (MR) are estimated when both shell side stream (sweep gas) and lumen side stream are continuously either in parallel flow configuration (co-current mode) or in counter-flow configuration (counter-current mode). Two mathematical models have been formulated and steady-state mass-balance gave two-dimensional differential equations, which were solved by using the orthogonal collocation technique. Simulation results for both co-current mode and counter-current mode have been compared in terms of hydrogen molar fraction (in the shell side) vs. axial co-ordinate at different hydrogen permeances, temperatures, and lumen pressures. At the operative conditions considered, a very similar CO conversion value has been obtained for both modes.

Keywords: Water gas shift; Theoretical model; Membrane reactor

1. Introduction

Several modelling works on membrane reactors (MRs) have been published in specialised literature for different chemical reactions, with particular regard to the feed mode of the lumen and shell side streams. For example, Becker et al. [1] formulated a two-dimensional mathematical model for catalytic dehydrogenation of ethylbenzene in a MR with parallel flow configuration. Itoh et al. [2–4] simulated the dehydrogenation of cyclohexane in a Pd-MR for both parallel flow and counter-flow reactor configurations. Mohan and Govind [5] studied the dehydrogenation of cyclohexane in a co-current. Casanave et al. [6] studied the dehydrogenation of isobutane in a packed-bed zeolite MR in both counter-current and co-current modes.

In the present work, the performance of the MR has been estimated with regard to the water gas shift reaction (WGSR):

$$CO + H_2O = CO_2 + H_2,$$
$$\Delta H^{\circ}_{298\,K} = -41.09\,kJ/mol$$

Both shell side stream (sweep gas) and lumen side stream are considered continuously in co-current mode or counter-current mode at the same operative conditions. The simulations referred to a Pd/Ag-based MR (effective length = 15 cm, membrane diameter = 1 cm) without defects on the surface in order to ensure infinite hydrogen selectivity with respect to other gases. The catalytic bed has been considered packed into the lumen side. The performance of the MR has been estimated changing the hydrogen permeance

* Corresponding author. Tel.: +39-0984-492011; fax: +39-0984-402103.
E-mail address: a.basile@itm.cnr.it (A. Basile).

0920-5861/$ – see front matter © 2003 Elsevier B.V. All rights reserved.
doi:10.1016/S0920-5861(03)00241-4

values, which practically could correspond to a thickness variation of the membrane considered. Simulations at different temperatures and lumen pressures have been performed for the counter-current mode; vice versa, different values of hydrogen permeance throughout the membrane have been considered for both modes.

2. MR modelling

A tubular configuration has been considered for the reactor working in isothermal conditions, at a fixed pressure of 100 kPa in the shell side. When the conversion is high, the longitudinal dispersion term can be significant in very short reactors and for low gas velocity (i.e. Reynolds number < 1) [7]. In this work, Reynolds number has been estimated in the range 10–15. Therefore, a total absence of axial mixing of the flowing streams within the reactor has been considered. Describing WGSR, a typical kinetic model has been assumed, Temkin's [8] model, and the following kinetic expression was adopted: $r\,(\mathrm{s}^{-1}) = k(p_{\mathrm{H_2O}}p_{\mathrm{CO}} - p_{\mathrm{H_2}}p_{\mathrm{CO_2}}/K_{\mathrm{eq}})(Ap_{\mathrm{H_2O}} + p_{\mathrm{CO_2}})^{-1}$.

The values of the parameters present in the above equation have been taken from literature [8].

Steady-state mass-balance gave two-dimensional differential equations for transport and reaction within the membrane module:

- Reaction side (lumen):

$$v_z\frac{\partial c_i}{\partial z} = \frac{1}{R}\frac{\partial}{\partial R}\left(RD_{i,R}\frac{\partial c_i}{\partial R}\right) + r_i$$

The boundary conditions (BC) are:

- BC 1: for each axial position (R=0), $\partial c_i/\partial R = 0$
- BC 2: for each axial position (R=d/2), $-D_{i,R}(\partial c_i/\partial R) = \mathrm{Pe}\left(\sqrt{p_{\mathrm{H_2,lumen}}} - \sqrt{p_{\mathrm{H_2,shell}}}\right)$
- BC 3: for each axial position (z=0), $c_i = c_{i,0\ \mathrm{lumen}}$

- Shell side:

$$v_z\frac{\partial c_i}{\partial z} = \frac{1}{R}\frac{\partial}{\partial R}\left(RD_{i,R}\frac{\partial c_i}{\partial R}\right)$$

The boundary conditions (BC) are:

- BC 4: for each axial position (R=d_r/2), $\partial c_i/\partial R = 0$
- BC 5: for each axial position (R=d/2), $D_{i,R}(\partial c_i/\partial R) = \mathrm{Pe}\left(\sqrt{p_{\mathrm{H_2,lumen}}} - \sqrt{p_{\mathrm{H_2,shell}}}\right)$
- BC 6: for each axial position (z=0), $c_i = c_{i,0\ \mathrm{shell}}$

where v_z is the axial velocity (cm/s), c_i the concentration of the species i in the mixture (mol/cm^3), $c_{i,0\ \mathrm{lumen}}$ the inlet concentration of the species i in the lumen side (mol/cm^3), $c_{i,0\ \mathrm{shell}}$ the inlet concentration of the species i in the shell side (mol/cm^3), $D_{i,R}$ the radial effective diffusivity for each species based on the total (void and non-void) area perpendicular to direction of diffusion (cm^2/s), z the axial co-ordinate (cm), d the diameter of the tubular membrane (cm), d_r the diameter of the MR (cm), R the radial co-ordinate (cm), r_i the reaction rate (mol/(cm^3 s)), $p_{\mathrm{H_2,lumen}}$ the hydrogen partial pressure in the lumen side (Pa), $p_{\mathrm{H_2,shell}}$ the hydrogen partial pressure in the shell side (Pa), and Pe the hydrogen permeance through the membrane (mol/(s cm^2 Pa$^{0.5}$)).

Different hydrogen permeance values have been considered, depending on thickness of the membrane used. In particular, the relationship between thickness and H_2 permeance is such that thickness' 0.68, 6.8, and 68 μm correspond to H_2 permeance of 2.56×10^{-3}, 2.56×10^{-4}, and 2.56×10^{-5} mol/(s m^2 Pa$^{0.5}$), respectively.

These equations have been solved using the orthogonal collocation technique. The same technique has been used by Hughes and co-workers [9,10], who studied the dehydrogenation of ethylbenzene using a two-dimensional mathematical model. This numerical solution procedure transforms the two-dimensional partial differential equations into total differential equations. In this way, a reactor can be modelled by a step-wise numerical procedure as the Runge–Kutta numerical method does. This procedure allows to predict reactor performances in terms of both axial and radial flows for each species. The model with parallel flow configuration is an initial value problem so it was possible to estimate hydrogen concentration in both sides of the MR proceeding in the same direction. The model with counter-flow configuration represents a boundary value problem so it was necessary to start by considering a hypothetical hydrogen concentration value at $z = 0$ in shell side. Repeating the calculations until convergence, the numerical code searches for the particular hydrogen concentration value that is zero at the end

of the reactor in shell side (that is the boundary condition).

3. Results and discussion

Simulation results in terms of molar fraction profiles for all reaction species (CO, CO_2, H_2O, and H_2) along the *z*-axis for counter-current and co-current modes are shown in Fig. 1. Operating conditions for the simulation tests are the following: $F_{CO,feed} = 1.17 \times 10^{-3}$ mol/min, $H_2O/CO = 1.5$, $T = 600$ K, $F_{N_2,sweep} = 1.65 \times 10^{-2}$ mol/min, $p_{lumen} = p_{shell} = 100$ kPa for both modes.

The main difference between the two operating modes concerns the hydrogen distribution in the shell and in the lumen. In particular, in the co-current mode (Fig. 1b) the hydrogen molar fraction in the shell

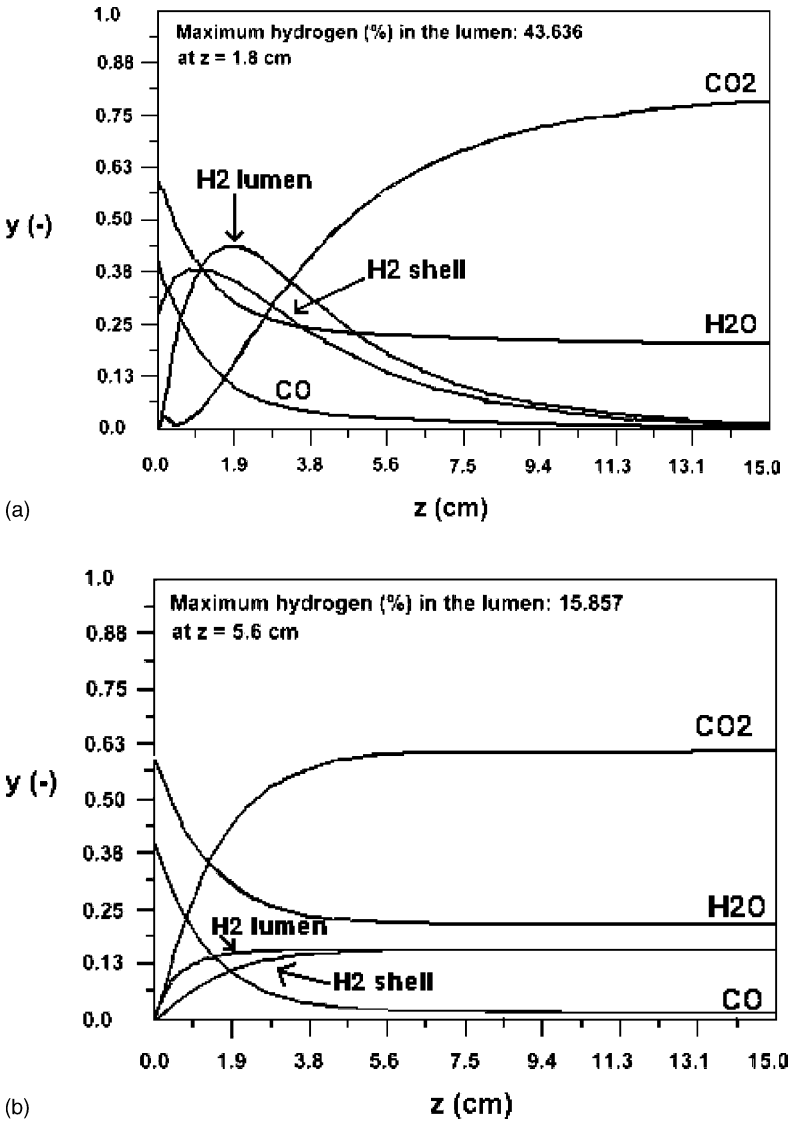

Fig. 1. Molar fraction of the reaction species vs. axial co-ordinate (membrane thickness = 0.68 μm): (a) counter-current mode; (b) co-current mode.

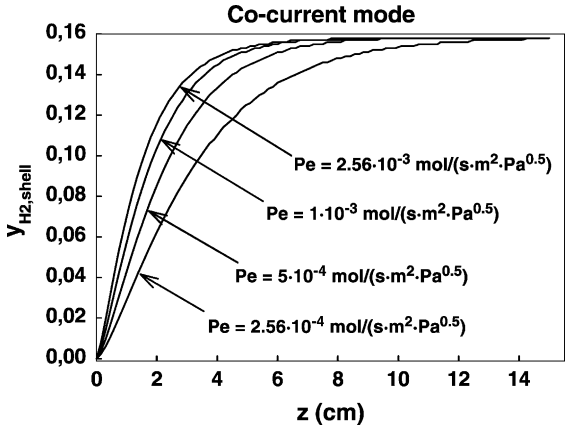

Fig. 2. Hydrogen molar fraction in the shell side vs. the axial co-ordinate at different hydrogen permeances through the membrane; co-current mode, $T = 600\,\text{K}$, CO conversion = 98.15%.

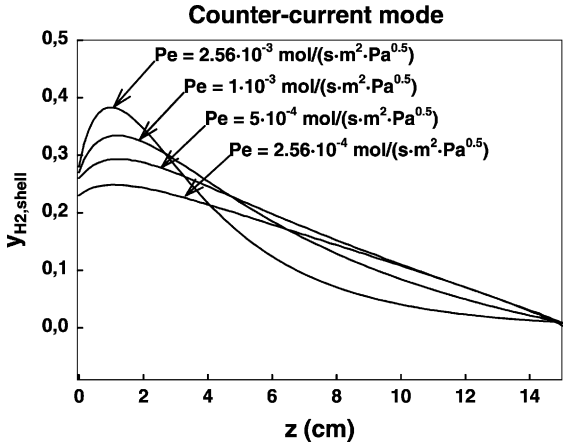

Fig. 3. Hydrogen molar fraction in the shell side vs. the axial co-ordinate at different hydrogen permeances through the membrane; counter-current mode, $T = 600\,\text{K}$, CO conversion = 100%.

approaches the hydrogen molar fraction in the lumen at the $z = 5.6\,\text{cm}$. Afterwards it keeps constant at 0.158. Hereinafter, the driving force for hydrogen permeation is practically zero, so no improvements due to the presence of the membrane are expected. Vice versa, in the counter-current mode (Fig. 1a) at $z = 0$ the hydrogen molar fraction in the shell (outlet side) is not zero ($y_{\text{H}_2,\text{out shell}} = 0.28$), while at $z = 15\,\text{cm}$ the hydrogen molar fraction in the lumen is zero (i.e. all the hydrogen produced in the lumen has been extracted). In this condition, the outlet stream of the lumen is practically without hydrogen, which is all permeated into the shell side.

Figs. 2 and 3 show simulation results in co-current and counter-current modes vs. axial co-ordinate, respectively, for different hydrogen permeance values. These figures show the variation of the hydrogen molar fraction in the shell side at the operative conditions investigated. A different behaviour is clearly shown. With regard to the co-current mode (Fig. 2), at a fixed axial co-ordinate, increasing the hydrogen permeance (i.e. by decreasing the membrane thickness) the hydrogen molar fraction in the shell side increases, due to the higher hydrogen flux through the membrane. Considering the counter-current mode (Fig. 3), the same trend is observed for $z < 3\,\text{cm}$. Moreover, the peak of hydrogen molar fraction becomes flat by decreasing the hydrogen permeance as well as the hydrogen molar fraction at the outlet of the shell side ($z = 0$) decreases.

At 600 K, thermodynamic equilibrium conversion of CO is 94.15%. In counter-current mode (Fig. 3), both a higher hydrogen permeance (e.g. $\text{Pe} = 2.56 \times 10^{-3}\,\text{mol/(s m}^2\,\text{Pa}^{0.5}\text{)}$) and an uniform driving force along the reactor have a slight positive influence on CO conversion with respect to the co-current mode (Fig. 2). In particular, CO conversion was 100% in the counter-current mode, vs. 98.15% achieved in the co-current mode.

At a lower hydrogen flow (e.g. $\text{Pe} = 2.56 \times 10^{-4}\,\text{mol/(s m}^2\,\text{Pa}^{0.5}\text{)}$) through the membrane, it is not possible to determine a significant difference in terms of CO conversion for the two modes. They seem quite equivalent in terms of CO conversion (96%).

The most important aspect to be considered in the comparison of the previous two figures is related to the driving force behaviour along the MR. Making our considerations in a general way by considering the hydrogen partial pressure instead of the hydrogen molar fraction, we can observe that:

(a) For the co-current mode (Fig. 2), the hydrogen driving force along the *z*-axis tends to zero, i.e. the hydrogen partial pressure in the shell side tends to reach the value of the hydrogen partial pressure in the lumen side. At the end of the MR, they are the same.
(b) Vice versa, for the counter-current mode (Fig. 3), the outlet side of the shell corresponds to the inlet side of the lumen (i.e. $z = 0$). In this case,

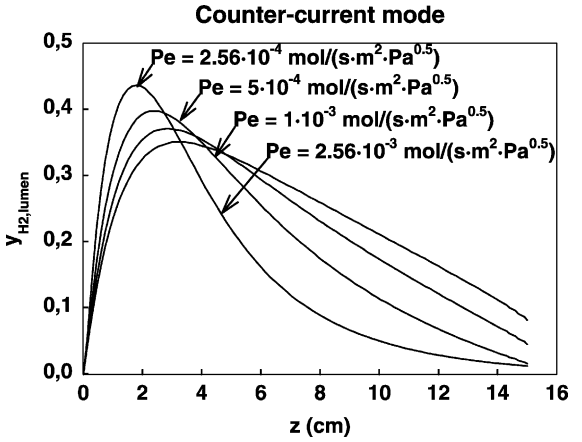

Fig. 4. Hydrogen molar fraction in the lumen side versus the axial co-ordinate at different hydrogen permeances through the membrane; counter-current mode.

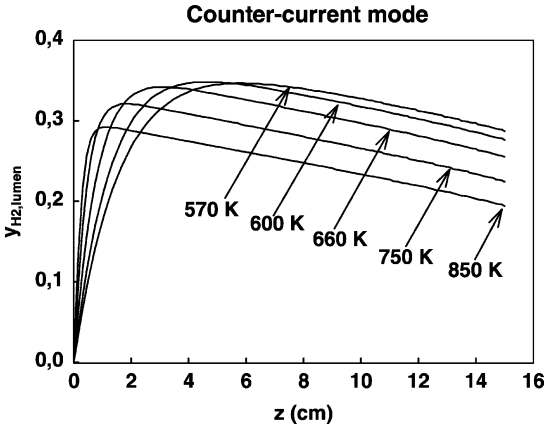

Fig. 5. Hydrogen molar fraction in the lumen side vs. the axial co-ordinate at different temperatures; counter-current mode.

the hydrogen partial pressure in the shell side overcomes the hydrogen partial pressure in the lumen, giving thereby a reverse hydrogen permeation from the shell side to the lumen side. So, in the first 2 cm of the reactor, from the inlet of the lumen ($z = 0$), this phenomenon inhibits the reaction (due to the Le-Chatelier principle, when a product is added to the reaction). This step justifies the same CO conversion achieved in the two modes at the lowest hydrogen permeance value (2.56×10^{-4} mol/(s m^2 Pa$^{0.5}$)). At the end of MR ($z = 15$ cm), the shell side contains sweep gas only, while in the lumen side the hydrogen partial pressure is lower than the hydrogen partial pressure in the shell side at $z = 0$ (Fig. 4). This aspect is very important when the hydrogen (or its isotopes such as deuterium and tritium) recovery is considered the main goal of the WGSR carried out in a MR [11,12].

Figs. 5 and 6 show the hydrogen molar fractions both in the lumen side and in the shell side, respectively, vs. the axial co-ordinate of the reactor in the counter-current mode, at different temperatures. Increasing the temperature, the hydrogen distribution in the lumen (Fig. 5) shows a maximum value closer to the inlet of the reactor. This maximum value decreases and shifts towards the inlet side of the reactor with the increasing temperature. This aspect could be explained by considering that when the temperature increases the hydrogen production rate increases (kinetic effect), while the reactants conversion decreases (due to thermodynamics). Moreover, increasing temperature results in an increase in the hydrogen permeation through the metallic membrane. Furthermore, due to the enrichment of hydrogen in the outlet stream of the shell side (from $z = 15$ cm to $z = 0$), the hydrogen molar fraction in the lumen side decreases from the value of z corresponding to the maximum to $z = 15$ cm. Vice versa, in the shell side (Fig. 6) the hydrogen molar fraction is practically the same at each temperature for a fixed axial co-ordinate. The maximum variation of hydrogen molar fraction in the shell side

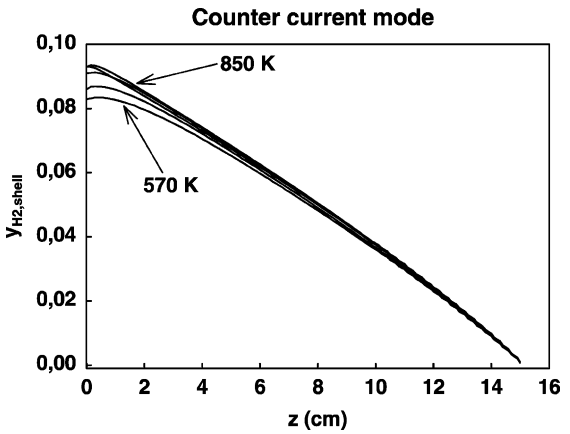

Fig. 6. Hydrogen molar fraction in the shell side vs. the axial co-ordinate at different temperatures; counter-current mode.

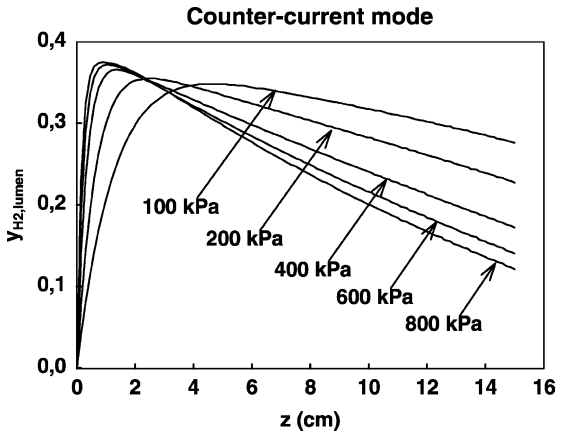

Fig. 7. Hydrogen molar fraction in the lumen side vs. the axial co-ordinate at different pressures; counter-current mode, $Pe = 2.56 \times 10^{-5}$ mol/(s m^2 Pa$^{0.5}$).

is shown at $z = 0$ in the shell side and corresponds to 0.08 (from 0.085 at 570 K to 0.093 at 850 K). Probably, in the shell side the temperature effect on hydrogen permeation contrasts with the lower hydrogen production in the lumen side (due to the exothermicity of the WGSR), so that the amount of hydrogen produced is lower than the hydrogen that could permeate.

Figs. 7 and 8 show the hydrogen molar fraction vs. axial co-ordinate at different reaction pressures in the lumen side and in the shell side of the reactor, respectively, in the counter-current mode. A very low

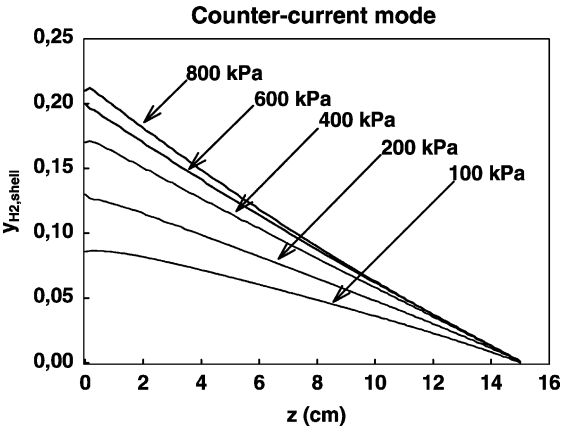

Fig. 8. Hydrogen molar fraction in the shell side vs. the axial co-ordinate at different pressures; counter-current mode, $Pe = 2.56 \times 10^{-5}$ mol/(s m^2 Pa$^{0.5}$).

Pe value is considered: 2.56×10^{-5} mol/(s m^2 Pa$^{0.5}$). The shell pressure is kept always constant at 100 kPa. Increasing the reaction pressure, the hydrogen distribution in the lumen (Fig. 7) shows a maximum value closer to the inlet of the reactor. This maximum value increases and shifts towards the inlet side of the reactor increasing pressure. This aspect could be explained by considering that when the pressure increases, the driving force for hydrogen permeation increases too: a major amount of hydrogen permeates through the membrane, while the non-permeated hydrogen remains into the lumen. Differently from the previous case related to the temperature effect (Fig. 6), hydrogen molar fraction in shell side (Fig. 8) changes at each reaction pressure for a fixed axial co-ordinate. This case shows how the driving force influences in a positive way the performances of the MR at 600 K.

4. Conclusions

The modelling analysis performed for both co-current and counter-current modes shows different hydrogen molar fraction profiles along the MR. However, from the point of view of CO conversion, both fluid-dynamic modes give the same value at low hydrogen permeance values. At high hydrogen permeance, the maximum difference in the two modes is about 2% in favour of the counter-current mode. The CO conversion is the same in both fluid-dynamic modes. Nevertheless, in the counter-current mode, a more uniform driving-force along the reactor is obtained. In the counter-current mode it is also possible to recover more hydrogen at the end of the reactor (outlet shell side) than in the co-current mode. Attention should be paid when the hydrogen recovery is more important than the CO conversion, for example when the hydrogen isotopes (such as deuterium and tritium) must be recovered during the WGSR carried out in a MR. In these cases, the counter-current mode is recommended with respect to the co-current one.

Acknowledgements

Authors wish to thank Mr. G. Chiappetta for his contribution in the realisation of the figures of the

paper. Special thanks to Mrs. America Oliva for improving the English of the paper.

References

[1] Y.L. Becker, A.J. Dixon, W.R. Moser, Y.H. Ma, J. Membr. Sci. 77 (1993) 233–244.
[2] N. Itoh, AIChE J. 33 (9) (1987) 1576–1578.
[3] N. Itoh, Y. Shindo, K. Haraya, J. Chem. Eng. Jpn. 23 (1990) 420–426.
[4] N. Itoh, W.C. Xu, K. Haraya, J. Membr. Sci. 66 (1992) 149–155.
[5] K. Mohan, R. Govind, AIChE J. 32 (12) (1986) 2083–2086.
[6] D. Casanave, P. Ciavarella, K. Fiaty, J.A. Dalmon, Chem. Eng. Sci. 54 (1999) 2807–2815.
[7] J. Smith, Chemical Engineering Kinetics, McGraw-Hill, New York, 1970.
[8] W.F. Podolski, Y.G. Kins, Ind. Eng. Chem. Process Des. Develop. 13 (4) (1974) 414–421.
[9] E. Gobina, K. Hou, R. Hughes, Chem. Eng. Sci. 50 (14) (1995) 2311–2319.
[10] E. Gobina, K. Hou, R. Hughes, Catal. Today 25 (3–4) (1995) 365–370.
[11] V. Violante, A. Basile, E. Drioli, Fusion Eng. Des. 30 (1995) 217–223.
[12] A. Basile, V. Violante, F. Santella, E. Drioli, Catal. Today 25 (1995) 321–326.